Int. J. Electrochem. Sci., 13 **(2018)** 1813 – 1821, doi: 10.20964/2018.02.23

International Journal of
ELECTROCHEMICAL
SCIENCE
www.electrochemsci.org

$PdCo_x$/rGO Nanocomposite Electrocatalysts Synthesized by Electrodeposition for Ethanol Electrooxidation in Alkaline Medium

Xiaowei Zhang, Yanhong Li, Jinlin Lu[*]*, Jidong Li, Lu Han, Yiyong Wang*

School of Materials and Metallurgy, University of Science and Technology Liaoning, Anshan 114051, P. R. China.
[*]E-mail: jinlinlu@hotmail.com

Received: 30 September 2017 / *Accepted:* 23 November 2017 / *Published:* 28 December 2017

In this article, a series of $PdCo_x$ metal catalysts deposited on graphene (rGO) as supporting materials were synthesized by electrodeposition. The composition and structure of the as-synthesized $PdCo_x$/rGO nanocomposite electrocatalysts were characterized by field emission scanning electron microscope, energy dispersive spectroscopy and Fourier transform infrared spectroscopy. Their electrochemical performances for ethanol electrooxidation were examined in alkaline medium. The results indicate that the compositions of the as-synthesized electrocatalysts are close to the metal ion concentration ratios in the precursors. The metal particle sizes of $PdCo_x$/rGO binary electrocatalys are smaller than the particle sizes of Pd/rGO and Co/rGO monometallic electrocatalysts. The $PdCo_{3.0}$/rGO electrocatalyst possesses the highest electrocatalytic activity and best stability for ethanol electrooxidation in alkaline environment.

Keywords: Electrocatalyst, Electrodeposition, Ethanol Electrooxidation, Graphene, Palladium

1. INTRODUCTION

Most of the energy consumed today is supplied from fossil fuels. It is now widely accepted that the increased combustion of fossil fuels has led to unprecedented changes in the chemical composition of Earth's atmosphere with multiple consequences for regional air quality and the global climate system. If today's entire surface traffic were powered entirely by fuel cell technology, anthropogenic emissions of the ozone precursors nitrogen oxide (NO_x) and carbon monoxide (CO) could be reduced by up to 50%, which would lead to significant improvements in air quality[1-6].

Ethanol is regarded as the best option in terms of lower toxicity, higher boiling point, lower vapor pressure and higher energy density. Direct ethanol fuel cells (DEFCs) generate electrical power

by feeding ethanol as fuel directly to an anode, which makes them easier to be designed as small and lightweight fuel cells[7]. DEFCs are attracting more and more attention as power sources for portable electronic devices and transportation due to the fact that ethanol possesses much higher energy density than gaseous fuels such as hydrogen and natural gas. Pt and Pt-based alloy electrocatalysts are widely investigated for ethanol electrooxidation[8-9]. However, the resources of Pt are sparse and its price is very high, especially, its tolerance to CO poisoning is very low, which significantly hinder the development of DEFCs. If DEFCs were operated in alkaline environments instead of acidic environments, the kinetics will be significantly improved and Pt-free electrocatalysts with low cost can be used[9-11]. Pd is a kind of noble metal with relatively low hydrogen over potential and good electrocatalytic activities for ethanol electrooxidation in alkaline environment. Many works have been done to enhance the electrocatalytic activities of Pd for ethanol electrooxidation[12-13].

Graphene (rGO) is a single-atom-thick sheet of hexagonally arrayed sp^2-bonded carbon atoms and is recently sparking great excitement in the scientific community given its excellent mechanical and electronic properties[14-20]. In this work, a series of $PdCo_x$ binary alloys with different Pd:Co ratios were co-electrodeposited on rGO. The as-prepared $PdCo_x$/rGO nanocomposites were applied as electrocatalysts for ethanol electrooxidation in alkaline media and their electrocatalytic activities and stabilities were investigated in detail.

2. EXPERIMENTAL

2.1 Materials

Materials used in this work include natural graphite flake, potassium permanganate, palladium chloride ($PbCl_2$), cobalt chloride ($CoCl_2$), ethanol, potassium hydroxide (KOH), phosphate buffer solution (PBS), aqueous ammonia were purchased from Sinopharm Chemical Reagent Co., Ltd. of China.

2.2 Preparation of $PdCo_x$/rGO

GO was prepared from the natural graphite by a modified Hummers method[21]. The detailed procedures can be found in our previous publications[22-23]. The preparation of the precursor solution for electrodepositing rGO on glass carbon electrode (GCE) is: 100 mg GO was added into 100 mL PBS solution with a concentration of 0.067 M and pH=9.18. The electrodeposition experiments were carried out using Autolab PGSTAT302N electrochemical workstation with a standard three-electrode cell. A GCE with a diameter of 4 mm was used as the working electrode, a platinum foil with 1 cm^2 as the counter electrode, and a saturated calomel electrode (SCE, 0.241 V *versus* standard hydrogen electrode) as the reference electrode. The electrodeposition experiments of rGO on GCE were performed by CV for 10 scan cycles from -1.5 V to 0.6 V in the nitrogen-purged precursor solutions with a scan rate of 50 mV s^{-1}. $PbCl_2$ and $CoCl_2$ with different molar ratios were added in deionized water to prepare the precursor solutions for fabricating Pd/rGO， $PdCo_{0.33}$/rGO， $PdCo_{1.0}$/rGO，

$PdCo_{3.0}$/rGO， Co/rGO electrocatalysts. The Pd^{2+} and Co^{2+} ionic concentrations were accordingly controlled as: 5 mmol L^{-1} Pd^{2+}, 5 mmol L^{-1} Pd^{2+} + 1.67 mmol L^{-1} Co^{2+}, 5 mmol L^{-1} Pd^{2+} + 5 mmol L^{-1} Co^{2+}, 5 mmol L^{-1} Pd^{2+} + 15 mmol L^{-1} Co^{2+} and 5 mmol L^{-1} Co^{2+}. The electrodeposition experiments of the different metal ions onto rGO were performed by CV for 20 scan cycles from -0.9 V to 0.9 V in the nitrogen-purged precursor solutions with a scan rate of 100 mV s^{-1}.

2.3 Characterization

Transmission electron microscopy (TEM) images were obtained using a JEOL 2010 electron microscope operated at 200 kV accelerating voltage with a cold-field emission source. Field emission scanning electron microscope (FESEM, JEOL JSM-6340F) was performed to characterize the morphology and the particle size distribution of the rGO on GCE and different $PdCo_x$/rGO electrocatalysts. EDS (Oxford, UK) was used to determine the composition of the electrocatalysts. Fourier transform infrared (FTIR) spectra were obtained using Agilent Technologies Cary 630 FTIR spectrometer at room temperature with a wave number range from 600 to 4000 cm^{-1}. The electrochemical measurements were carried out in a conventional three-electrode cell using the Autolab PGSTAT302N at ambient temperature.

3. RESULTS AND DISCUSSION

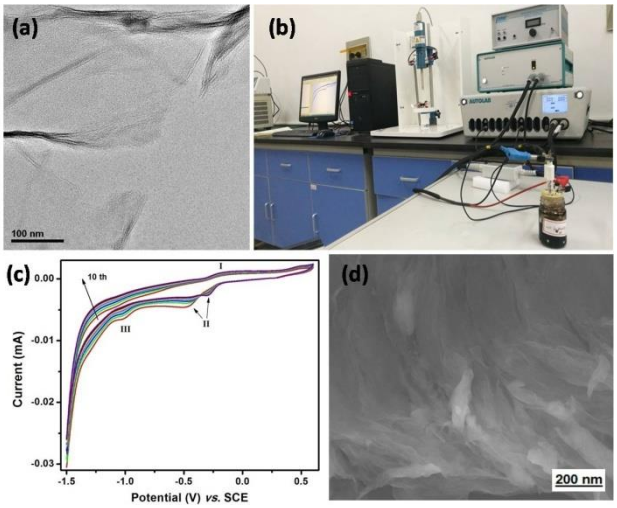

Figure 1. (a) TEM image of GO dispersed in PBS solution, (b) the setup for the electrochemical experiments, (c) CV curves for electrodepositing rGO on GCE, (d) FESEM image of rGO on GCE.

Figure 1a displays the isolated GO sheets extracted from the PBS solution, which corroborates that GO can form well-dispersed and exfoliated structure in the PBS solution. Figure 1b is a photo presenting the setup for the electrochemical experiments in our laboratory. Figure 1c shows a set of CV curves with 10 scan cycles for electrodepositing rGO on GCE. The scan range is from -1.5 V to

0.6 V and scan rate is 10 mV s^{-1}. The pair of anodic peak (I) and cathodic peak (II) can be attributed to the redox of some electrochemically active oxygen-containing groups on graphene planes that are very stable in this potential range[20]. With increasing the scan cycle number, the peak II shift positive slightly. The cathodic peak (III) at the potential of ~-1.0 V are attributed to the irreversible electrochemical reduction of GO. The formation of rGO film on the GCE can be easily confirmed by the FESEM image as shown in Figure 1d. The rGO film shows a typical wrinkled sheet structure, which would be useful as scaffold for electrodeposition of metal nanoparticles[24].

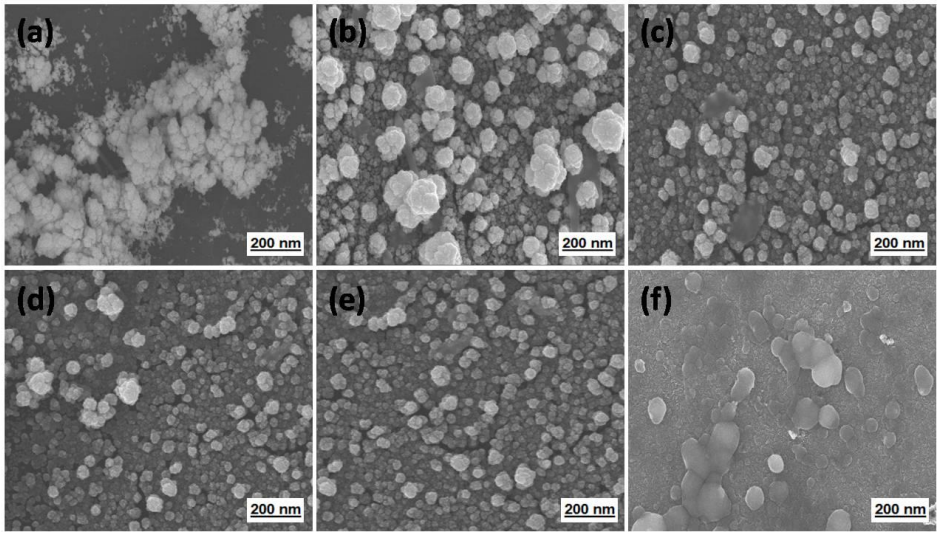

Figure 2. FESEM images of (a) Pd/GCE, (b) Pd/rGO, (c) $PdCo_{0.33}$/rGO, (d) $PdCo_{1.0}$/rGO, (e) $PdCo_{3.0}$/rGO and (f) Co/rGO.

Figure 2 shows the morphologies of metal electrocatalysts with different Pd:Co molar ratios synthesized by the electrodeposition process. As can be seen from Figure 2a, there is an obvious agglomeration phenomenon for the pure Pd metal particles deposited on blank GCE surface. However, the pure Pd metal particles deposited on rGO/GCE shows uneven particle size distribution without obvious agglomeration phenomenon as shown in Figure 2b. It may contribute to the strong anchoring effect between the Pd nuclei and the graphene surfaces[25]. In comparison with Pd/rGO, the three different PdCo binary nanocomposites exhibit relatively even particle size distribution as shown in Figure 2(c-e). The particle sizes are about ranging from 10~90 nm. The pure Co tended to form a dense film on rGO.

Figure 3a shows the EDS diagrams of the different electrocatalysts. The Pd/rGO and Co/rGO exhibit the characteristic peaks of their corresponding elements. The $PdCo_{0.33}$/rGO, $PdCo_{1.0}$/rGO and $PdCo_{3.0}$/rGO have the characteristic peaks of both Pd and Co elements. Moreover, the corresponding elemental compositions of the different binary electrocatalysts detected by EDS are quite close to the original composition in the precursor solution. The results demonstrate that the Pd and Co elements were stoichiometrically codeposited on rGO surfaces by the electrodeposition process. Figure 3b shows the FTIR spectra of the different samples. The spectrum of pristine GO illustrates the presence

of C-O ($\nu_{C\text{-}O}$ at 8422 cm^{-1}), C-O-C ($\nu_{C\text{-}O\text{-}C}$ at 980 cm^{-1}), C-OH ($\nu_{C\text{-}OH}$ at 1065 cm^{-1}), and C=O in carboxylic acid and carbonyl moieties ($\nu_{C=O}$ at 1721 cm^{-1}).

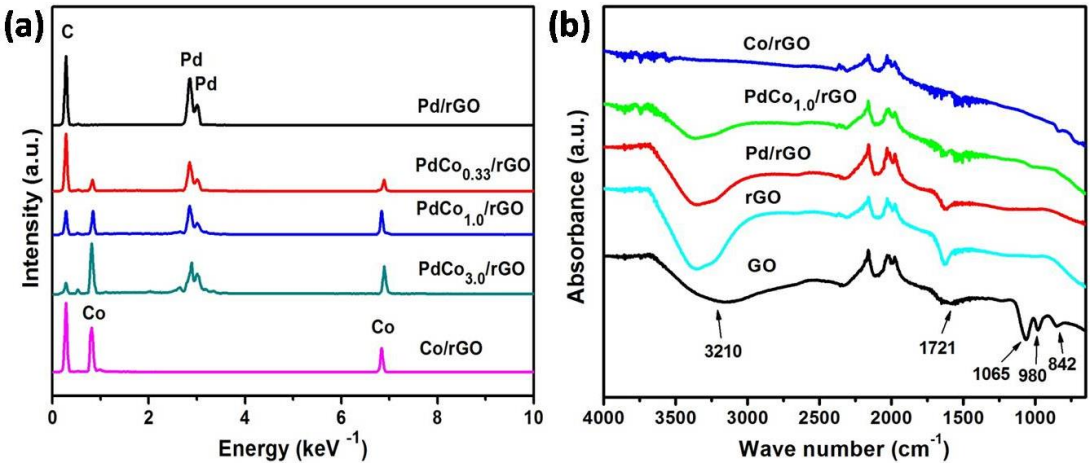

Figure 3. (a) EDS diagrams of the different electrocatalysts, (b) FTIR spectra of the different samples.

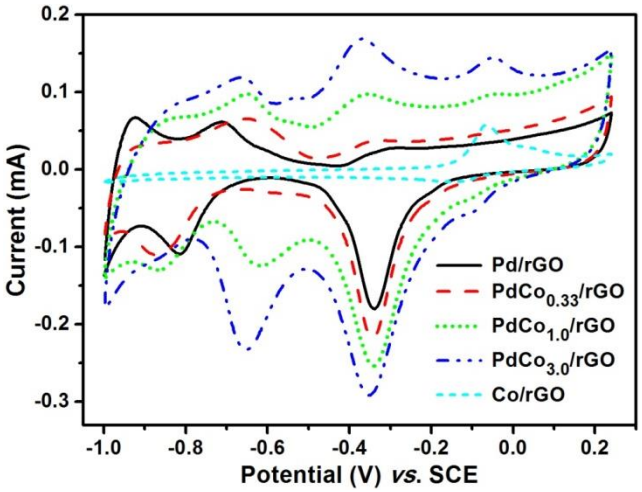

Figure 4. (a) CV curves of the different electrocatalysts in N_2-saturated 1.0 M KOH solution.

However, the peaks of C=O at ~1721 cm^{-1} still exist in the pure rGO and the other composite electrocatalysts. The results indicate that the GO molecules have not been completely reduced by the electrodeposition process[9-20], which is in good agreement with the CV results (Figure 1c).

The CV results of the different electrocatalysts in 1.0 M KOH solution are presented in Figure 4. The scan rate is 50 mV s^{-1} and the scan range is from -1.0~0.24 V. The monometallic Pd/rGO electrocatalyst has the corresponding hydrogen desorption and adsorption peaks in the range of -1.0~-0.6 V via the following reactions[8]:

$$Pd\text{-}H_{ads}+OH^{-} \rightarrow Pd+H_2O+e^{-} \quad (1)$$

$$Pd+H_2O+e^{-} \rightarrow Pd\text{-}H_{ads}+OH^{-} \quad (2)$$

The anodic peak of Pd/rGO emerged at the potential of ~-0.3 V can be attributed to the formation of PdO layer. The process can be explained as follows:

$$Pd+OH^- \rightarrow Pd\text{-}OH_{ads}+e^- \quad (3)$$

$$Pd\text{-}OH_{ads}+OH^- \rightarrow Pd\text{-}O+ H_2O+e^- \quad (4)$$

$$Pd\text{-}OH_{ads}+ Pd\text{-}OH_{ads} \rightarrow Pd\text{-}O+ H_2O \quad (5)$$

The cathodic peak of Pd/rGO emerged at the potential of ~-0.33 V can be attributed to the reduction of PdO to Pd. The process can be explained as follows[26]:

$$Pd\text{-}O+H_2O+2e^- \rightarrow Pd+2OH^- \quad (6)$$

For the monometallic Co/rGO electrocatalyst, no hydrogen desorption and adsorption peak was observed, but a pair of peaks at ~-0.08 V and -0.14 V were observed clearly. These peaks can be ascribed to the redox of Co as well and the similar features have been reported in KOH electrolyte. The process can be explained using the following reaction steps:

$$Co+OH^- \rightarrow Co\text{-}OH_{ads}+e^- \quad (7)$$

$$Co\text{-}OH_{ads}+OH^- \rightarrow Co\text{-}O+ H_2O+e^- \quad (8)$$

$$Co\text{-}OH_{ads}+ Co\text{-}OH_{ads} \rightarrow Co\text{-}O+ H_2O \quad (9)$$

$$Co\text{-}O+H_2O+2e^- \rightarrow Co+2OH^- \quad (10)$$

All the binary nanocomposite electrocatalysts exhibit bigger hydrogen adsorption/desorption region. The electrochemical active surface area (ECSA) can be measured by integrating the charge in the reduction of Pd oxide and can be calculated according to the following equation[26]:

$$ECSA = \frac{Q}{SL}$$

where Q denotes the Coulombic charge of PdO reduction, L is the loadings of Pd catalyst, and S is the conversion factor with the value of 405 μC cm^{-2}.

The electrocatalytic activities and stabilities of the different electrocatalysts for ethanol electrooxidation were examined by CV and CA tests accordingly. The reaction kinetics parameters of the different electrocatalysts including onset potential (E_s), peak potential (E_p), peak current density in anodic scan (j_p) are listed in Table 1.

Table 1. Electrochemical parameters of different electrocatalysts for ethanol electrooxidation in alkaline medium.

Electrocatalysts	E_s (V)	E_p (V)	j_p (mA cm^{-2})	I_f/I_b
Pd/rGO	-0.66	-0.26	63	0.9
$PdCo_{0.33}$/rGO	-0.69	-0.25	68	1.0
$PdCo_{1.0}$/rGO	-0.70	-0.24	84	1.2
$PdCo_{3.0}$/rGO	-0.72	-0.15	170	1.3
Co/rGO	-	-	-	-

The currents are normalized with the GCE area. As presented in Figure 5a, ethanol starts to be oxidized from about -0.7 V during the forward scan. The higher j_p is, the higher catalytic activity the catalyst has. Obviously, the $PdCo_{3.0}$/rGO has the highest catalytic activity for ethanol electrooxidation and its j_p is nearly 3 times higher than that of monometallic Pd/rGO. The Co/rGO doesn't demonstrate any catalytic activity. But with increasing the Co content, the j_p of the binary catalysts increases

significantly and the E_s shifts negatively, which indicates an improvement in the catalytic activity and kinetics. The results corroborate that the Co content has a great impact on the catalytic activity and reaction kinetics for ethanol electrooxidation. Some literatures also reported the effects of Co elements on ethanol electrooxidation in alkaline media. The results demonstrated that the incorporated Co facilitated the oxidation of strongly adsorbed carbonaceous intermediate species on the surface of Pd by forming OH^- group and reacts away the intermediated from Pd surface.

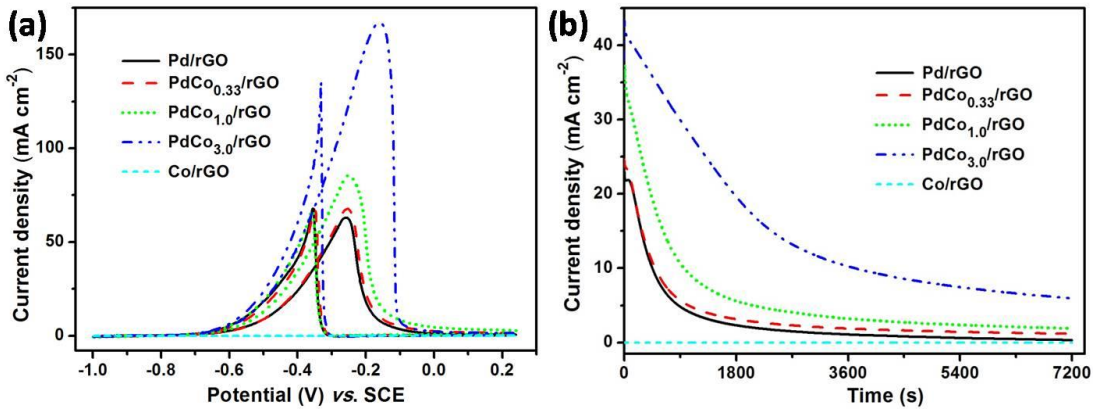

Figure 5. (a) CV and (b) CA results of the different electrocatalysts in N_2-saturated 1.0 M KOH + 1 M CH_3CH_2OH solution.

Table 2. Comparison of some similar electrocatalysts reported.

Catalysts	Supporting materials	Method for preparing catalysts	Activities ($mA\ cm^{-2}$)	Ref.
$Pd_{100}Co_{10}$	Polyvinylpyrrolidone	Electrodeposition	142	12
Pd_1Co_2	Carbon	Reduction by $NaBH_4$	23	13
NiCo	Graphene	Reduction by $N_2H_4{\cdot}H_2O$	17	14
$PdCo_{3.0}$	Graphene	Electrodeposition	168	This paper

It is well known that there are still two major limitations: splitting C-C bonds and removal of strongly adsorbed carbonaceous intermediates such as $(CH_3CO)_{ads}$[27-28]. In the backward scan, the sharper peaks can be ascribed to the removal of carbonaceous species not completely oxidized during forward scan. The peak current ratio I_f/I_b (forward peak current density)/(backward peak current density) can be used to express the carbonaceous tolerance of electrocatalysts. As can be seen from Table 1, the I_f/I_b values of the binary electrocatalysts are all bigger than that of Pd/rGO, demonstrating the enhanced carbonaceous tolerance on $PdCo_x$/rGO catalysts. The significantly enhanced electrocatalytic performances should be due to the synergistic catalytic effect between Pd and Co elements[29-30]. The stabilities of the different electrocatalysts for ethanol electrooxidation were investigated in 1.0 M KOH + 1.0 M ethanol solution by CA method at a constant potential of -0.3 V and the results are shown in Fig 5b. The current densities of all the electrocatalysts decrease very fast in the initial testing period. The rapid current decays are mostly caused by the poisoning effect of carbonaceous intermediates formed during ethanol electrooxidation reaction. The Pd/rGO catalyst displays the fastest current reduction among these catalysts, indicating the lowest tolerance to

carbonaceous intermediates. On the contrast, the current density of $PdCo_{3.0}$/rGO is always the highest in these catalysts. The good stability of $PdCo_{3.0}$/rGO can be attributed to the quick removal of the adsorbed carbonaceous intermediates on the catalyst surfaces[31-33]. This is a very interesting and important implication for the development of DEFC.

4. CONCLUSIONS

In brief, a facile and simple method through two-step electrodeposition was used to synthesize the $PdCo_x$/rGO nanocomposite electrocatalysts. It can be seen that graphene as a catalyst support is very beneficial to fabricate highly dispersed nanoparticles. The significant enhancements of electrochemical performances of the binary electrocatalysts towards ethanol electrooxidation are due to the introduction of Co elements, which can provide the required hydroxide ions for oxidizing and removing residual carbon species on Pd catalyst surfaces. The introduction content of Co elements is a key parameter to influence the electrochemical performances of the binary electrocatalysts. And the excellent electrochemical performances of the $PdCo_{3.0}$/rGO electrocatalyst demonstrate that it is a promising electrocatalyst for developing alkaline DEFCs.

ACKNOWLEDGEMENT
This work was supported by the National Natural Science Foundation of China (NO. 51774177, 51674141, 51504133), Project of Liaoning Province Department of Science and Technology (20170540468), Liaoning BaiQianWan Talents Program (2017-104), Innovative Research Team Funding of University of Science and Technology Liaoning (No. 2016TD05).

References

1. S.Y. Wang, S.P. Jiang, *Natl. Sci. Rev.*, 4 (2017) 163-166.
2. J. Lu, H. Tang, S. Lu, H. Wu, S.P. Jiang, *Journal of Materials Chemistry*, 21 (2011) 6668-6676.
3. J. Lu, S. Lu, S.P. Jiang, *Chemical Communications*, 47 (2011) 3216-3218.
4. L. Wu, S.K. Zhong, F. Lv, J.Q. Liu, *Materials Letters*, 110 (2013) 38.
5. Y. Zhou, X.C. Hu, X.H. Liu, H.R. Wen, *Chem. Commun*., 51 (2015) 15297.
6. Y. Zhou, X.C. Hu, Q.Z. Fan, H.R. Wen, *J. Mater. Chem*. A., 4 (2016) 4587.
7. Y. Wang, S.Z. Zou, W.B. Cai, *Catalysts*, 5 (2015) 1507-1534.
8. H.Q. Ji, M.G. Li, Y.L. Wang, F. Gao, *Electrochem. Commun*., 24 (2012) 17-20.
9. J.D. Cai, Y.Y. Huang, Y.L. Guo, *Appl. Catal. B-Environ*., 150 (2014) 230-237.
10. F.F. Ren, H.W. Wang, C.Y. Zhai, M.S. Zhu, R.R. Yue, Y.K. Du, P. Yang, J.K. Xu, W.S. Lu, *ACS Appl. Mater. Interfaces*, 6 (2014) 3607-3614.
11. K.I. Ozoemena, *RSC Adv*., 6 (2016) 89523-89550.
12. Z.S. Yang, J.J. Wu, *Fuel Cells*, 12 (2012) 420-425.
13. S. Han, G.S. Chae, J.S. Lee, *Korean J. Chem. Eng*., 33 (2016) 1799-1804.
14. Z.H. Wang, Y.L. Du, F.Y. Zhang, Z.X. Zheng, Y.Z. Zhang, C.M. Wang, *J. Solid State Electrochem*., 17 (2013) 99-107.
15. M.S. Ahmed, S. Jeon, *ACS Catal*., 4 (2014) 1830-1837.

16. R.P. Xiu, F.F. Zhang, Z.H. Wang, M. Yang, J.F. Xia, R.J. Gui, Y.Z. Xia, *RSC Adv*., 5 (2015) 86578-86583.
17. C.T. Hsieh, J.M. Wei, J.S. Lin, W.Y. Chen, *Catal. Commun*., 16 (2011) 220-224.
18. M.M. Zhang, Z.X. Yan, Y. Li, J.J. Jing, J.M. Xie, *Electrochim. Acta*, 161 (2015) 48-54.
19. K. Wu, Q. Zhang, D.M. Sun, X.S. Zhu, Y. Chen, T.H. Lu, Y.W. Tang, *Int. J. Hydrog. Energy*, 40 (2015) 6530-6537.
20. Z.H. Xue, B. Yin, M.Q. Li, H.H. Rao, H. Wang, X.B. Zhou, X.H. Liu, X.Q. Lu, *Electrochim. Acta*, 192 (2016) 512-520.
21. W.S. Hummers Jr, R.E. Offeman, *Journal of the American Chemical Society*, 80 (1958) 1339.
22. J.L. Lu, Y.H. Li, S.L. Li, S.P. Jiang, *Sci Rep*, 6 (2016) 12.
23. J.L. Lu, W.S. Liu, H. Ling, J.H. Kong, G.Q. Ding, D. Zhou, X.H. Lu, *RSC Adv*., 2 (2012) 10537-10543.
24. L.Y. Chen, Y.H. Tang, K. Wang, C.B. Liu, S.L. Luo, *Electrochem. Commun*., 13 (2011) 133-137.
25. M. Asnavandi, B.H.R. Suryanto, C. Zhao, *RSC Adv*., 5 (2015) 74017-74023.
26. R. Kiyani, S. Rowshanzamir, M.J. Parnian, *Energy*, 113 (2016) 1162-1173.
27. N. Alfi, A.R. Rezvani, M. Khorasani-Motlagh, M. Noroozifar, *New J. Chem*., 41 (2017) 10652-10658.
28. A. Santasalo-Aarnio, E. Sairanen, R.M. Aran-Ais, M.C. Figueiredo, J. Hua, J.M. Feliu, J. Lehtonen, R. Karinen, T. Kallio, *J. Catal*., 309 (2014) 38-48.
29. X. Tarrus, M. Montiel, E. Valles, E. Gomez, *Int. J. Hydrog. Energy*, 39 (2014) 6705-6713.
30. H. Erikson, A. Sarapuu, J. Kozlova, L. Matisen, V. Sammelselg, K. Tammeveski, *Electrocatalysis*, 6 (2015) 77-85.
31. A. Serra, E. Gomez, I.V. Golosovsky, J. Nogues, E. Valles, *J. Mater. Chem*. A, 4 (2016) 7805-7814.
32. J.L. Lu, Z.H. Li, S.P. Jiang, P.K. Shen, L. Li, *Journal of Power Sources*, 202 (2012) 56-62.
33. E.D. Park, D. Lee, H.C. Lee, *Catalysis Today*, 139 (2009) 280-290.